Dripwater organic matter and trace element geochemistry in a semi-arid karst environment

Rutlidge, Helen; Baker, Andy; Marjo, Christopher E.; Andersen, Martin S.; Graham, Peter W.; Cuthbert, Mark O.; Rau, Gabriel C.; Roshan, Hamid; Markowska, Monika; Mariethoz, Gregoire; Jex, Catherine N.

DOI:
10.1016/j.gca.2014.03.036

Dripwater organic matter and trace element geochemistry in a semi-arid karst environment: implications for speleothem paleoclimatology

Helen Rutlidge,[a,b,g*] Andy Baker,[b,g] Christopher E. Marjo,[a] Martin S. Andersen,[c,g] Peter Graham,[b] Mark O. Cuthbert,[c,d] Gabriel C. Rau,[c,g] Hamid Roshan,[c,g] Monika Markowska,[b,e,g] Gregoire Mariethoz,[b,g] Catherine Jex[b,f,g]

[a] Solid State and Elemental Analysis Unit, Mark Wainwright Analytical Centre, The University of New South Wales, Kensington, NSW, Australia 2052

[b] Connected Waters Initiative Research Centre, The University of New South Wales, Kensington, NSW, Australia 2052

[c] Connected Waters Initiative Research Centre, The University of New South Wales, 110 King Street, Manly Vale, NSW 2093, Australia

[d] School of Geography, Earth and Environmental Sciences, University of Birmingham, Edgbaston, Birmingham, B15 2TT, UK

[e] Australian Nuclear Science and Technology Organisation, Lucas Heights NSW 2234, Australia

[f] Water Research Centre, The University of New South Wales, Kensington, NSW, Australia 2052

[g] Affiliated to the National Centre for Groundwater Research and Training, Australia

* Corresponding author. Tel.: +612 9385 9327; fax: +612 9385 3327.

E-mail address: a.baker@unsw.edu.au

Abstract

A series of four short-term infiltration experiments which revealed hydrochemical responses relevant to semi-arid karst environments were carried out above Cathedral Cave, Wellington, New South Wales (NSW), Australia. Dripwater samples were collected at two sites for trace element and organic matter analysis. Organic matter was characterised using fluorescence and interpreted using a PARAFAC model. Three components were isolated that represented unprocessed, soil-derived humic-like and fulvic-like material, processed humic/fulvic-like material and tryptophan-like fluorescence. Principal Component Analysis (PCA) performed on the entire dataset comprising trace element concentrations and PARAFAC scores revealed

two dominant components that were identified as soil and limestone bedrock. The soil component was assigned based on significant contributions from the PARAFAC scores and additionally included Ba, Cu, Ni and Mg. The bedrock component included the expected elements of Ca, Mg and Sr as well as Si. The same elemental behaviour was observed in recent stalagmite growth collected from the site. Our experiments demonstrate that existing paleoclimate interpretations of speleothem Mg and Sr, developed in regions of positive water balance, are not readily applicable to water limited environments. We provide a new interpretation of trace element signatures unique to speleothems from water limited karst environments.

1. Introduction

Trace elements are preserved in speleothem calcite and are increasingly used either in chronology (where trace elements vary rhythmically; Smith et al., 2009) or as a paleoclimate proxy (Sundqvist et al., 2013; Wassenburg et al., 2013). Trace elements can derive directly from precipitation; from biogeochemical reactions between recharge and trace elements associated with organic matter, colloids, clays and bedrock clasts within the overlying soil; and from biogeochemical reactions between infiltration water and trace elements associated primarily with the limestone bedrock overlying the cave (Fairchild et al., 2000; Fairchild and Treble, 2009; Tremaine and Froelich, 2013). Therefore trace element composition of waters infiltrating into a cave can be a product of many processes which include metal-organic matter binding (Borsato et al., 2007; Hartland et al., 2012), soil cation exchange, incongruent and congruent dissolution of bedrock and soil clasts (Hansen and Postma, 1995), and the amount of prior calcite precipitation (PCP). Variable soil water residence times (related to climatic conditions) and degrees of mixing between recently infiltrated precipitation, existing older soil water, and vadose zone water may lead to variable elemental compositions for elements that are released by kinetically controlled reactions, such as weathering of primary silicate minerals (Appelo and Postma, 2005). Regardless, the trace element distribution in speleothem deposits will be related to the infiltration water geochemistry and further modified during calcite precipitation. For full reviews, we refer the reader to Fairchild and Treble (2009), Fairchild and Baker (2012) and Tremaine and Froelich (2013).

Trace elements have been widely investigated in speleothem paleoclimatology because they can give insights in the multitude of processes that determine infiltration. However they have yielded quantifiable paleoclimate proxies in only a limited number of cases. The majority of

research has focussed on Mediterranean, temperate and alpine climatic regions, where mean annual precipitation (*P*) is typically greater than mean annual evapotranspiration (*ET*). Pioneering initial research by Roberts et al. (1998) demonstrated annual variability in Sr/Ca, Mg/Ca and Ba/Ca in a temperate climate Scottish speleothem. Fairchild et al. (2000) demonstrated that variations in water availability, which control the extent of prior calcite precipitation (PCP) and incongruent dissolution of bedrock could be the primary controls on speleothem Sr/Ca and Mg/Ca, and this has been recently demonstrated through the investigation of many diverse sites by Tremaine and Froelich (2013). In drier conditions, there is longer water residence time in the epikarst leading to decreased drip rates and enhanced CO_2 degasing. This system results in higher Mg/Ca and Sr/Ca ratios than those found in congruent dissolution of limestone due to preferential removal of Ca (Tremaine and Froelich 2013). Organic matter associated trace elements have also been recognised which include, P, Cu, Pb, Zn and Y (Borsato et al., 2007), and have been associated with infiltration events that mobilise soil organic matter and colloids (Hartland et al., 2012). Where trace element variations occur regularly, such as in climate regions with strong seasonality, high resolution (sub-annual) analysis of these trace elements in speleothems provides an annual chronology (Smith et al., 2009), which has been successfully used to provide high precision records of past climate (for example, Sundqvist et al., 2013).

Although karst infiltration water trace element geochemistry increasingly is well understood, the majority of research has been undertaken in temperate to alpine environments, where on average mean annual $P>ET$. In these environments, soil organic matter is relatively abundant, soil geochemistry is primarily controlled by weathering of the underlying bedrock, and infiltration and associated speleothem deposition can be considered to be relatively continuous (Fairchild and Baker 2012). These conditions contrast those in more arid environments: where $P<ET$, soil organic matter may be limited and the soil is poor in nutrients such as phosphorus. In these regions evaporation processes dominate over infiltration, leading to salt accumulation within the soil profile (McDonald et al., 2007). With increasing aridity, aeolian processes and dust deposition becomes an increasingly important contributor to the soil geochemical profile (Greene et al., 2009). Soil trace element geochemistry therefore depends on the interplay between the extent of soil salinisation (controlled by *ET*), the proximity of potential dust sources, a site climatology that permits dust transport and deposition, the soil organic matter content and character, and the bedrock geochemistry. Infiltration events are irregular, often without an annual frequency.

Consequently speleothem deposition, and thus trace elemental composition, can be considered to be episodic rather than seasonal. In a pioneering study in SE Australia, McDonald et al. (2007) presented 5-yrs of trace metal data from cave dripwater and noted a more complex response of dripwater Mg/Ca, Sr/Ca and Ba/Ca to climate than observed in temperate regions. More recently, Frisia et al. (2012) demonstrated that the P record preserved in Australian speleothems could be both a function of within-cave microbial processes as well as soil-derived infiltration. However, despite these two studies, review of available literature indicate that karst infiltration processes in arid and semi-arid zones are rarely investigated and thus require further research.

In this paper we present the results of an infiltration experiment performed at the Wellington Caves, NSW, Australia. We undertook an artificial infiltration experiment to better understand the trace element geochemistry of dripwaters in semi-arid climate regions where $P<ET$. We believe that this is the first such experiment undertaken to understand karst dripwater trace element composition. Furthermore, water sampling comprised both inorganic elements (trace metals) and dissolved organic matter analysis by fluorescence, permitting the investigation of the association of organic matter with trace elements. Our results are relevant to the interpretation of speleothem trace element records from any arid or semi-arid regions where infiltration events are infrequent and evaporation dominates the soil water balance. This of course includes modern day semi-arid and arid climate regions, as well as regions which have experienced past aridity in the Quaternary or older time periods. Our results will therefore facilitate the interpretation of speleothem trace element records from regions such as Israel (Bar Matthews et al., 1991), Yemen (Van Rempelbergh et al., 2013), Turkey (Siklósy et al., 2009) and Morocco (Wasserburg et al., 2013), as well as from Australia (McDonald et al., 2007).

2. Study site

The Cathedral Cave in Wellington, NSW, Australia is located at 32 37'S; 148 56'E, in a temperate semi-arid climate (Figure 1c), with mean annual precipitation of 619 mm (1956-2005) and evaporation of 1825 mm (1965-2005) recorded at the nearby Wellington Research Centre (Australia Bureau of Meteorology). There is a significant seasonal temperature variation with monthly mean maximum ranging from 15 °C in July and 32 °C in January (1956-1990, Australia Bureau of Meteorology). The limestone bedrock geology has been described previously as a mixture of massive and thinly-bedded Devonian limestone

(Johnson 1975). The site of this study is within the massive limestone, with a red-brown soil comprising clays, iron oxides, fine quartz sands, and calcite nodules (Frank, 1971), with aeolian contributions (Hesse and McTanish, 2003).

Wellington is situated within a region where dryland salinity occurs. Dryland salinity is often due to deforestation over the last 200 years, which results in the saline groundwater entering the soil by capillary action and subsequent evaporation resulting in the accumulation of salts. Regional soils are ubiquitously affected by aeolian dust deposition, with current estimates ranging from 13 – 50 t km^{-2} a^{-1} in southeast Australia (Green et al., 2009). Potential dust sources are diverse, and include distal arid climate sources such as Lake Eyre, and proximal sources from deflation of alluvial material in the Murray-Darling Basin (Hesse and McTanish, 2003).

The geomorphology of Cathedral Cave has been extensively researched (Osborne, 2007) and has abundant evidence of hypogene formation processes in addition to conventional meteoric water features, arguably typical of many caves in SE Australia (Osborne, 2010). The cave has been a focus of long-term hydrogeological monitoring (concurrent to this study) by the investigators, commencing in 2010 and continuing, primarily using a network of in-situ Stalagmate © drip loggers. Mariethoz et al. (2012) utilised near-surface infiltration to identify non-linear and chaotic drip behaviour and its relationship to surface connectivity. Jex et al. (2012) described infiltration patterns and processes within the cave, and identified that infiltration only occurs after high magnitude and duration rainfall events, with a total precipitation of over ~60mm within 24-48 hours, however the necessary amount of rainfall needed can vary dependant on antecedent conditions. Such rainfall events occur very infrequently, typically 0-2 times a year, and require slow-moving weather systems. In winter, this is mostly likely associated with westerly frontal rainfall, where the associated low pressure system is slow moving, deep, and relatively close to the site. In summer, instability and associated convective rainfall caused by slow moving or stationary troughs and associated upper level systems, draws moist, unstable air from the north of the region. These previous investigations have identified a section of the cave that had numerous near-surface, intermittent dripping sites (see Figure 1a). Our irrigation experiment was therefore located above this section of the cave, and the two dripwater sites reported here were designated as Sites 1 and 2 (Figure 1b).

3. Methods

3.1 The irrigation experiment

In this study, an area, of approximately 3 × 7 m, directly above the study area in Cathedral Cave was irrigated with Wellington town supply water. The experiment was done in the height of the Australian summer and the antecedent soil moisture was very low (soil moisture was measured at the nearby Wellington Research Centre as 0.1 weight fraction at the time of the study). Two Monsoon pumps were used to distribute the irrigation water from a 1600 L tank. The irrigations were carried out over a period of two hours each morning, for four consecutive days from the 8th January 2013. The volume and size of the irrigation area was chosen to achieve equivalent of more than 60 mm of rainfall over the irrigation site. Infiltration events were designated 1 to 4 with the following volumes: Event 1: 840 L (start time 7:00 am Day 1), Event 2: 1500 L (start time 8:00 am, Day 2), Event 3: 840 L (start time 8:00 am, Day 3), Event 4: 1500 L (start time 6:00 am, Day 4). The irrigation on Day 1 was spiked with 0.5 L of 99.8 % deuterium (D_2O) into 840 L of town water. The resulting deuterium enrichment was 6100 ‰ (VSMOW) as measured by laser cavity ring down analysis (see below). For reference the tank water was sampled at the beginning and end of each irrigation (for chemical composition see Supporting data table S1).

3.2 Cave dripwater sampling

The onset and rate of inflow to the cave was monitored at three stalactites using Stalagmate © drip loggers located under drip sites on the cave floor. Water samples were collected below the drip loggers in a plastic funnel which was mounted at ~30 cm height from the cave floor using commercial drainpipe. The base of the funnel drained into 1L HDPE water sample collection bottles (Supporting data Figure S2a). Two of these drip sites activated during the irrigation, and cave dripwater samples were collected from Sites 1 and 2 for trace element; fluorescent organic matter analysis; and electrical conductivity (EC) measurements. Three other sites also activated in close proximity (within 0.2 m either side) of Sites 1 and 2, but sampling was not possible due to either uneven floor surface or proximity to Sites 1 and 2. Water samples were collected regularly from the 1 L sample containers during day time. A subsample of ~20 ml was used for EC measurements on site using a HACH HQ40d multimeter and EC probe. When drip rates were slow, samples from Site 1 and 2 were mixed in equal proportions to permit enough sample volume for EC analysis. For this reason EC was not included in the PCA analysis. Subsamples for trace element and fluorescence analysis were collected in 30 mL PET containers. 30 mL water samples for water isotope

analysis were collected in glass McCartney bottles. Therefore, all were integrated samples: initial sample collection was at 30 minute intervals, reducing to hourly intervals during the recession phase of each event. When dripping continued overnight, the sampling interval was increased. A ~5 mL aliquot from the 30 mL PET container was filtered (0.45 μm PSE filters) and analysed for organic matter fluorescence at the nearby UNSW Wellington Field Station within 24 hrs. The remainder of the sample was refrigerated for up to one week, transported in a coolbox to the UNSW Analytical Centre, Sydney, and filtered (0.45 μm PSE filters), acidified (100 μL of concentrated HNO_3 to 10 mL of sample) ready for trace element analysis. Isotope samples were sealed, stored and kept in the dark at room temperature until analysis.

3.3 Cave dripwater analysis

Trace-element analysis of the dripwater samples (without dilution) was carried out using a Perkin Elmer NexION 300D ICP-MS and Perkin Elmer Optima 7300 ICP-OES. The following elements were analysed by ICP-OES: Ca, Mg, Si and Sr, and by ICP-MS: Al, Ba, Cu, Fe, Ni, P, Pb, U and Zn (Supporting data Table S2 and S3). For both techniques multi-element standards in 2% nitric acid were prepared from 1000 mg l^{-1} single element stock solutions (High-Purity Standards^{TM}). Standards were prepared at the following concentrations for ICP-OES, 0.2, 1, 10, and 100 mg l^{-1} and at 0.2, 1, 10 and 100 μg l^{-1} for ICP-MS analysis. Of these, the following elements were considered reliable for interpretation Ca, Mg, Si, Sr, Ba, Cu, and Ni. P and Pb were below the detection limit (10 μg l^{-1} and 0.10 μg l^{-1} respectively) of the ICP-MS and the other excluded elements exhibited a high proportion of outliers that would skew the subsequent PCA. A single spike in the Cu results was removed from the data on the basis that there was no corresponding spike observed in any other elemental data.

Organic matter characterisation was undertaken using fluorescence spectroscopy. A Horiba Aqualog fluorescence spectrometer was used, which measures both absorbance and fluorescence within the same instrument, with the absorbance data used to correct for any reabsorption (or inner-filter) effects. Fluorescence excitation-emission matrices (EEMs) were collected using an excitation range of 240 to 400 nm, with a step-size of 3 nm, and emitted fluorescence detected between 210 and 600 nm with a CCD detector, at a spectral resolution of 1.64 nm and integration time of 1 s. All data was inner-filter corrected, scatter lines

masked, and Raman normalised (to a mean Raman intensity of water in a sealed water cell, excited at 380 nm, of 200 intensity units), using proprietary Aqualog software. The resultant dataset of 83 EEMs was analysed using parallel factor analysis (PARAFAC) using Eigenvector Research Solo © software. The PARAFAC method models the resulting data cube and extracts fluorescence components. Standard checks (split-half analysis, core consistency analysis, the presence of physically meaningful components) were applied to the resultant models to ensure model integrity (Stedmon and Bro, 2008). This resulted in a three component PARAFAC model being adopted.

The trace element concentrations and the PARAFAC scores were analysed by PCA for each individual site. PCA was performed in the PLS toolbox (Eigenvalue Research, Inc.) with the data auto-scaled prior to the analysis.

Water isotopic composition of irrigation and dripwater samples was determined using an LGR-24 d off-axis, integrated cavity output, cavity ringdown mass spectrometer (ICOS CRMS, Lis et al., 2007, Wassenaar et al., 2008) at the University of New South Wales. Analytical precision was 0.1 per mil (1σ; calculated from within run internal references materials).

3.4 Soil and rock analysis

A limited sampling of the soil and bedrock was performed at the site. A single limestone sample from the bedrock at an accessible exposure at the edge of the irrigation area was collected, and a single soil sample was obtained approximately 30 cm below the soil surface from within the centre of the irrigated area (Figure 1a). The soil and rock samples were analysed to determine their mineralogy and elemental composition. Cave rock samples were crushed to a ca. 20 micron powder in a tungsten-carbide ring mill. Soil samples were prepared by drying for 3 hours at 90 °C, followed by grinding to a ca. 20 micron powder in a mortar and pestle. The powdered samples were used for XRD analysis. Analysis for major and trace elements was performed by preparing a glass bead using 1:10 weight percent of the powdered sample in a 12:22 lithium metaborate flux (Norrish and Hutton, 1969). The resulting bead was analysed for the major elements using a Panalytical PW2400 wavelength dispersive XRF Spectrometer fitted with a rhodium anode end window X-ray source and calibrated using glass beads prepared from the Panalytical WROXI element set and processed using the Panalytical SuperQ software. Semi-quantitative trace element analysis was

conducted on the prepared glass bead using laser ablation ICPMS on a New Wave NWR213 laser ablation unit coupled to a Perkin Elmer NexION 300D ICP-MS and calibrated using the NIST 612 silicate glass standard.

X-ray diffraction of soil and rock samples was performed on a PANalytical MPD diffractometer fitted with a Pixel array detector and a copper anode X-ray source. Measurements were performed between 5° and 70° with a step size of 0.001 2θ whilst spinning the sample. All powders were side-loaded into stainless steel sample holder for analysis. Diffraction data was processed using the PANalytical HighScore Plus software to remove artefacts from copper Kβ radiation, baseline-corrected using a polynomial function, then fitted to a series of pseudo-Voigt functions to obtain the peak areas. A single calcite phase was identified in the cave rock sample. In the soil samples low angle peaks at 9.95 Å, 9.01 Å, 7.10 Å supported the presence of illite, smectite, and kaolinite clays, along with strong diffraction form a quartz phase. A semi-quantitative analysis was performed using the clay 090 reflection (62.1° 2θ, 1.49 Å) and the neighbouring quartz 211 reflection (60.0° 2θ, 1.54 Å) based on reliability of the 090 peak for clay quantitation, and the absence of overlap with other peaks (Środoń et al., 2001). Semi-quantitation of the diffracting mineral phases was performed using a standard addition of quartz (20 wt%), and then the resulting mineral phase composition adjusted to include an amorphous (non-diffracting) phase of iron oxide/hydroxide identified in the XRF measurements.

3.5 Stalagmite collection and analysis

The cave area below the irrigation site is in a public section of the cave and hence stalagmite collection was not possible. However sampling was possible away from the public section in a hydrologically active area known as South Passage, which is approximately 30-40 m from the infiltration site and approximately 20 m deeper (Figure 1a) and within the monitoring network reported by Jex et al. (2012), where drip rates generally increase 10 – 20 days after rainfall. We therefore conceptualize that stalagmites in this area are subject to the same parent hydrochemistry as Sites 1 and 2. A stalagmite was collected from South Passage in 2011. The trace element record was measured along the growth axis on one half of the cut stalagmite by a New Wave NWR213 laser ablation unit coupled to a Perkin Elmer NexION 300D ICP-MS. Elemental data was collected continuously with a 25 µm spot size and a scan speed of 25 µm s^{-1}. The following elements were analysed Ba, Cu, Mg, Ni, P, Si and Sr and reported relative to Ca and converted to semi-quantitative data using NIST612 silicate glass

standard. PCA was performed on the stalagmite data using PLS toolbox (Eigenvalue Research, Inc.) after the data were auto-scaled.

4. Results

4.1 Soil and rock mineralogy and elemental composition

A subset of relevant results for the XRF and LA ICPMS elemental analysis of the soil and rock samples are given in Table 1, and the complete analysis is given in the Supporting data Table S4. From these results it appears that Mg is present at similar levels in the soil and in the bedrock, and Ba is only detectable in the soil sample. The soil sample contains a high level of Si. P is only detected in the soil, presumably associated with organic matter. The majority of the limestone bedrock sample comprised of calcite, with trace quantities of other minerals, including quartz. The soil was found to be a mixture of kaolinite, illite, and smectite (bentonite) clays (56%) that have been reported at this site (Frank, 1971, Gingele et al., 2005), quartz (15%), and iron oxides (7%), with 20-22% volatiles.

4.2 Drip rates and dripwater stable isotope time series

The time series of drip rate and stable isotopes of the cave dripwater during the four days of the short-term irrigation experiment above Cathedral Cave are plotted in Figure 2. On Day 1, no dripwater was observed at any of our drip samplers, including Sites 1 and 2. Therefore, we hypothesise that the irrigation water was primarily held in the overlying soil. On Day 2, three hours after the start of irrigation Event 2, dripping was observed at Sites 1 and 2 for a period of two hours and peaking at rates of 8.25 mL min^{-1} for Site 1 and 2.95 mL min^{-1} for Site 2. On Day 3, following irrigation Event 3, dripping restarted at Sites 1 and 2 2.5 hours after irrigation commenced and peaked at rates of 12.10 mL min^{-1} for Site 1 and 10.20 mL min^{-1} for Site 2. Site 1 then dripped continuously while Site 2 dripping ceased after 17.5 hours. On Day 4, after irrigation Event 4, Site 1 continued to drip and dripping restarted at Site 2 one hour after the start of the irrigation. Rates peaked at 11.55 mL min^{-1} for Site 1 and 6.15 mL min^{-1} for Site 2. Both sites were monitored for a further 24 hours, during which time both sites continued to drip.

The irrigation water on Day 1 was spiked with deuterium and used as an artificial tracer of water movement and to permit a calculation of the dilution of cave dripwater with respect to the irrigation water. Isotope analysis of the dripwater samples (Figure 2) demonstrated that an increase above the background natural variability of deuterium (−9.2‰ vs −15.8‰) was not

observed until the end of dripping on Day 2 with the maximum value of +11.5‰ reached on Day 3 and then steadily decreasing until the end of monitoring on Day 4 to values of about −4‰, still above the natural background level.

4.3 Trace element analysis

Figure 2 shows the dripwater EC and selected elemental concentration changes over time for Site 1 and 2. Every elemental plot is characterised by certain features. The dripwater EC data generally started out high for each event with EC ranging from 430-493 µS cm^{-1} for Site 1 and 430-488 µS cm^{-1} for Site 2, depending on the day. As drip rates decreased the EC decreased to between 406-430 µS cm^{-1} for Site 1 and 406-466 µS cm^{-1} for Site 2, depending on the day. For most elements (Figure 2) the initial dripwater sample, collected on Day 2, had high relative concentrations suggestive of initial flushing of ions during the first flow. Subsequent samples on Day 2 showed a rapid decrease in concentrations, with the exception of Si. Elemental concentrations on Day 3 showed an initial high concentration similar to that observed initially on Day 2. This initial peak was smaller for Ba and Mg compared to the initial peak on Day 2. Day 3 behaviour was repeated on Day 4 though on a smaller scale. When the rate of dripping reduced, all trace element concentrations increased with the exception of Ca (and EC), which decreased. Over the period of the experiment, Si and Sr show an upward trend at both sites. Within each site Cu and Ni show very similar behaviour over the period of the experiment. However, when comparing these elements between sites a notable difference is the lack of a concentration spike on Day 4 for Site 1. Ba also shows a difference between the two sites, with a concentration spike present on Day 3 at Site 2 and Day 4 at Site 1.

4.4 Organic matter analysis

For the organic matter analysis, PARAFAC indicated that a three factor model provided realistic excitation and emission spectral profiles and appropriately modelled the data. The three factors were identical to those widely reported as the most common factors in fluorescence EEMs from a wide range of aquatic environments (Stedmon et al., 2003; Dainard and Guéguen, 2013). These three factors are characterised following Ishii and Boyer (2012). Factor 1 fluoresces at relatively long emission wavelengths (peak centred at 460 nm) and is commonly identified as unprocessed, soil-derived humic-like and fulvic-like material that has a high aromaticity and/or molecular weight. Factor 2 fluoresced at a shorter emission

wavelength (peak centred at 400 nm) and is commonly identified as biogeochemically processed humic/fulvic-like material, where aromatic structures have been bio- or photo-degraded, with a resulting structure that is less aromatic and/or has lower molecular weight. Factor 3 fluoresced in the short UV (peak centred at 340 nm) that is associated with living or dead microbial matter (tryptophan-like fluorescence) and is therefore indicative of microbiological activity (Hudson et al 2008). We hypothesise that all of the factors are soil-derived given the 0-0.3 m thickness of soil overlying the infiltration site and a bedrock thickness of 1.7-3 m limiting the likelihood of other sources of organic matter between the soil surface and the drip sites.

The PARAFAC score for each factor (which provides a quantitative measure of fluorescent dissolved organic matter (fDOM) for each component) is shown in Figure 3. Similar to the trace element data on Day 2, each factor had an initial high amount of fDOM followed by a rapid decrease suggestive of initial flushing. On the subsequent days the amount of fDOM levelled out, peaking in the middle of Day 3 and 4 for Factors 1 and 2, potentially related to time of maximum soil moisture.

4.5 Trace element and DOM PCA

For each site an individual PCA was performed on the entire dataset, comprising the trace element concentrations and PARAFAC scores (representing the organic matter). For both sites, the first two components account for approximately 70% of the variance in the dataset. The contribution of each variable in the analysis is given in Table 2. The most notable observation about component 1 in both sites is the contribution of the PARAFAC scores with the concentrations of Ba, Cu, Mg, and Ni. The presence of the PARAFAC scores in component 1 (but not component 2) suggests that component 1 represents soil-derived material. Component 2 has significant contributions from Ca, Mg, and Sr for both sites, cations that are typically derived from limestone bedrock, and in addition Si. These elemental assignments are supported by the soil and bedrock elemental results, as Mg was present at similar levels in the soil and bedrock component and Ba only detected in the soil sample. However, despite PCA suggesting that the dissolved Si is a bedrock-derived element, it was present at a high level in the soil sample. Further discussion of the Si results is found in section 5.

406 The score plot for the soil and bedrock component is given in Figure 4 for Site 1 and 2. Both
407 components show evidence of an initial flushing on Day 2, however the soil component is
408 significantly higher indicating a higher proportion of elements and organics in that fraction.
409 On the subsequent days the level of the soil component remains relatively consistent,
410 however the daily average bedrock component increases. The reasons for this behaviour are
411 unclear but might be attributed to longer residence time or to contributions from zones not
412 activated on the previous days.
413
414 **5. Discussion**
415 Prior to the experiment the soil surface above the cave was dry and there were no active drip
416 sites, which is generally the case for the site. Dripping only activates after major rain events
417 of more than about 60 mm, although this depends the on antecedent conditions of the soil
418 (Jex et al., 2012). In this area of the cave, dripping will only last for a maximum of two
419 weeks in accordance with the semi-arid conditions of the site. The residual soil moisture is
420 immobile for long periods of time between events and able to equilibrate with minerals and
421 organic material in the soil. The flow path on the cave wall below the exfiltration point is
422 observed to dry up between rain events to presumably leave traces of dissolved salts and
423 organic matter. Evidence of organic matter deposition can be seen by the discolouration along
424 the flow paths (see Figure S2b). This could explain the high concentrations of both trace
425 element and organic components during the first flush on the second day of the experiment.
426 Also, it was seen albeit to a smaller degree on the subsequent days, indicating that the system
427 was continually wetting up during the entire experiment. A conclusion supported by the more
428 sustained dripping on subsequent days.
429
430 During this study, the drip rates for Site 1 were consistently higher than for Site 2 and had a
431 longer recession on Day 3 (Figure 2) and at the end of dripping after Event 4 (not shown).
432 However, the longer recessions at Site 1 only corresponded to a small additional volume, for
433 example on Day 3 there was an additional 96 ml at Site 1 after dripping stopped at Site 2. We
434 believe the small differences in the hydrology of the two sites are due to the flow paths for
435 Site 1 and 2 only diverging within the cave (see Figure S2b). During periods of high drip
436 rates all sites are activated (additional dripping was observed at three adjacent sites). As the
437 drip rate slowed the outer flow paths dry up and dripping ceased at these sites, with Site 1
438 having a longer recession as it appears to be supplied by the central flow path.
439

The hypothesis that the irrigation water was initially held in the overlying soil is supported by the morphology of the site and the deuterium results. The area irrigated was 3 x 7 m with a continuous thin surface soil layer that we estimate to generally vary between 0-0.3 m. However, additional soil is present at deeper levels in fractures in the underlying bedrock. From these figures the estimated the soil volume is 2.1 – 6.3 m^3 equivalent to 3.8 – 11.3 tonne of soil (assuming bulk density of 1.8 g ml^{-1}). The soil moisture records (November 2011 to May 2013) from the nearby Wellington Research Station indicate a soil moisture capacity of up to 0.6 wfw, and the existing soil moisture was 0.1 wfw. Hence a conservative estimate of the soil's additional water storage capacity is approximately 1890 – 5670 l supporting the hypothesis that the 840 l of water from Event 1 was stored initially in the soil. In addition, the appearance of an increase above the background natural variability of deuterium in the dripwater confirms that the water from Day 1 was initially stored in the overlying soil. Since this increase was not observed until the end of dripping on Day 2 this demonstrates that the initial cave dripwater on Day 2 was stored water from before the irrigation experiment, pushed into the cave by the applied irrigation water, and that the irrigated water did not start to appear until the end of dripping on Day 2, with the majority of the irrigation water appearing on Day 3.

The deuterium data permits an estimation of dilution of the irrigation water (in the tank) with pre-existing soil and vadose zone water. The deuterium value measured for the irrigation water on Day 1 was 6100‰ and the maximum deviation from the background of the collected dripwater samples was ~27‰ at Site 1 and ~25‰ at Site 2. Using these values the minimum dilution of the irrigation water was 0.45%. When this dilution factor is applied to the elemental concentrations of the irrigation water, the measured elemental cave dripwater concentrations are several orders of magnitude higher for all elements and organic component scores (values are given Supporting data table S1). This is an important observation as it demonstrates that the organic or elemental signature of the water used for the irrigation does not need to be considered further and validates the use of the artificial irrigation to investigate contributions of soil and bedrock to the chemistry of cave dripwaters.

In absolute terms the collected dripwater cation inorganic chemistry is dominated by the dissolved Ca with concentrations ranging between 73 and 94 mg l^{-1}, as would be expected in this system. When comparing to the EC values using the condition that the sum of cations (on a milli-equivalent basis) should equal EC/100 (in µS cm^{-1}), Ca explains between 90-100% of

the dissolved cation load. Interestingly, both EC and Ca are observed to decrease when drip rates are decreasing towards the end of each day (Figure 2). We hypothesise that this due to slower flow on the cave features which allows more time for dissolved CO_2 to equilibrate and degas to the cave atmosphere. This process could be driving PCP and explain the decrease in Ca and consequently EC. Unfortunately, this hypothesis could not be tested by calcite saturation calculations since the experimental setup and collected sample volumes did not allow for alkalinity analysis and reliable pH measurements.

It was somewhat surprising that the PCA grouped dissolved Si with the limestone bedrock trace elements since the total element analysis demonstrated that Si was of significantly greater abundance in the soil than found in the bedrock (Table 2). This can be explained by the generally dry nature of the site, and hence the relatively long water residence times in the soil between infiltration events that allow weathering reactions in the soil to reach conditions where Si concentrations are controlled by the equilibrium of precipitating secondary minerals. Si concentrations therefore are controlled by equilibrium conditions rather than by kinetically controlled weathering of primary silicate minerals (Appelo and Postma, 2005). This is supported by the concentrations of Si and dissolved aluminium (Table S2 and S3), which are consistent with equilibrium conditions for kaolinite (observed in the soil) at a reasonable soil pH ca 4.8. Likewise Si concentrations are observed in a very tight range 5.4-6.1 which is in the concentration range observed for equilibrium with a SiO_2(s) solid somewhere in the range between quartz and amorphous SiO_2(s) (Appelo and Postma, 2005). We hypothesise that the narrow observed range of Si is due to equilibrium control in the soil. We further hypothesise that the PCA grouping of Si with the limestone bedrock trace elements could be due to the frequent precipitation and re-dissolution of Si on the cave features along the flow path related to the drying and wetting events.

5.1 Sr and Mg in dripwater

In a review of dripwater Sr and Mg trace element concentrations from diverse cave research monitoring campaigns, Tremain and Froelich (2013) concluded that Sr/Ca and Mg/Ca in dripwaters and stalagmites are likely to be useful indications of groundwater residence time at sites where there was a single source of Sr and Mg (e.g. bedrock). Where this was stable over time, Sr/Ca and Mg/Ca could be used as paleoclimate proxies, and the stability could be tested through the analysis of the Sr/Mg ratio in stalagmites over time. Following the work of Fairchild et al. (2000) Tremain and Froelich (2013) clearly demonstrated that for sites where

precipitation dominates over evaporation, PCP is the dominant process that controls dripwater and stalagmite Sr and Mg.

Figure 5 presents Sr/Ca vs Ca and Mg/Ca vs Ca for the three days of the infiltration experiment. Due to the short duration of the experiments, we expect PCP would be limited during the initial stages of infiltration, but would increase as drip rates slow and residence time increases. Overall, we would hypothesise that the evolution of Ca, Sr/Ca and Mg/Ca over time would be dominated the interplay between rapid dissolution of carbonate minerals, and any subsequent prior calcite precipitation, assuming a single bedrock source of Mg and Sr. Figure 5a and b demonstrates that this is the case, with increasing Ca concentration between Days 2, 3 and 4, a strong correlation between Ca and Sr/Ca during each drip event, and with no significant change in Sr/Ca ratio between the drip events. However, Figure 5c and d demonstrates a complex response, both within individual irrigation events and between events. The complex behaviour of Mg results in extensive scatter in the Sr/Ca versus Mg/Ca plot (Supporting data Figure S4) that precludes the use of this type of plot to identify PCP by divergence from the mixing radial as demonstrated by Tremaine and Froelich 2013. The difference in dripwater Sr and Mg responses during the irrigation events reflects the relative geochemistry and mineral solubility of the soil and bedrock at our site (Table 2). Whereby, soil geochemistry dominated by silicates and bedrock chemistry by carbonates, and a similar abundance of magnesium in both the soil and bedrock when analysed as total elemental composition.

At our site, in a region where loess contributes to the soil and salt accumulation within the soil profile is expected to occur (Hesse and McTainsh, 2003), Mg fails the ‘single source’ test of Tremaine and Froelich (2013). Instead, Mg accumulation occurs in the soil due to evaporation, the relatively low proportion of Mg in the Devonian Limestone limits its signature from the bedrock, and there is a relatively low contribution of regolith derived Mg to the soil geochemistry at a site where dust deposition is frequent. Our observations are made at an event scale, and the extent to which they apply at seasonal inter-annual timescales needs further investigation. It is possible, that over long-time periods, PCP may become a more dominant, and the Mg signature might be dominated by this process. We consider this further in section 5.3.

5.2 Soil and bedrock trace element signatures in dripwater

Potentially, Sr is identified as a useful trace element signature of bedrock contact time over the scale of individual irrigation events, typical of the occasional high rainfall amount events that generate groundwater recharge at our research site. At the timescale of individual recharge events, dripwater Sr concentration is dominated by dissolution. The Sr appeared in the PCA as component 2, along with Si and Ca (Table 2, Figure 4), and component 2 had a negative correlation with fDOM, indicating that this was a grouping of bedrock-derived trace elements.

Dripwater PCA analysis demonstrates that trace elements which can be uniquely attributed to being soil-derived are Ba, Ni, and less conclusively Cu. Both Ni and Cu have been previously recognised as organo-colloid associated trace elements (Borsato et al., 2007; Hartland et al., 2012) and their association with fDOM is expected. Ba has been previously interpreted as a bedrock-derived trace element due to its ability to replace calcium in octahedrally-coordinated lattice positions within $CaCO_3$ (Fairchild et al., 2010). However, Ba was undetectable in the Devonian limestone sample, but found in the soil. Given the high solubility of barium in water and acids, and its strong absorption by clay minerals, we hypothesise our clay-rich soils provide the dominant source of Ba and it is therefore a soil signature. McDonald et al. (2007), sampling dripwaters at Wombeyan Caves, 250 km to the SE, found that Ba concentrations did not represent water residence times in the bedrock.

Therefore we hypothesise that Ba and organo-colloid associated trace elements such as Ni and Cu provide trace element signatures of soil and only Sr provides a signature of the bedrock, at least over event timescales. At our temperate semi-arid site, long term and frequent aeolian deposition to the land surface has formed a silicate and clay rich soil which can strongly bind Ba (Eylem et al., 1990), and provides a source of Si. Soil-derived dripwater contains high concentrations of fDOM and associated metals with a high binding affinity. The concentrations of Si, also a soil-derived element at this site, is controlled by the equilibrium of the precipitation of secondary silica minerals. Where water is in contact with the bedrock, Sr should be increasing with time. Over longer than event timescales, dripwater Sr concentration will also be controlled by PCP. This suggests that Mg in the environment of this study is a poor tracer as it has potential sources from soil salt accumulation due to the high *ET*, a potential source in high Mg clays weathered from aeolian deposition, and a limestone dissolution source. In addition, Mg will vary with the degree of PCP within the bedrock above the cave. This suggests it may be necessary to investigate and interpret the

trace element response to recharge on a site-by-site basis to calibrate these proxies in stalagmites. To test these hypotheses, we consider the recent stalagmite trace element record from the cave.

5.3. Recent stalagmite trace element profile.

An actively-forming stalagmite from South Passage was sampled in 2011 and the top 2.6 mm analysed using LA-ICPMS. Although the exact growth rate for this sample is not known, speleothems in this part of the cave have deposited over infrastructure installed in 1926 when it was the show cave. A total speleothem accumulation of 22 mm is indicative of a minimum growth rate of 0.26 mm yr^{-1}. This is in agreement with that expected for the observed dripwater Ca concentrations of 70-90 mg l^{-1} (Figure 2) (Dreybrodt, 1999). Therefore we hypothesise that the top 2.6 mm represents the last 10 years of deposition. The stalagmite is situated around 20 m below the site affected by the irrigation experiment. Jex et al. (2012) demonstrated that drip rates in this part of the cave increases 10 to 20 days after long-duration, high volume rainfall events, and dripping is maintained for several weeks to years, depending on the flow path. We hypothesise that the dripwater from this section of the cave has the same parent hydrochemistry as dripwater from the irrigation events and it has likely to have undergone PCP.

Figure 6 presents the LA-ICPMS data for Mg, Si, Sr, Cu, P and Ba, normalised to Ca for the stalagmite and Figure 7 shows the loading plot for component 1 versus component 2 from the PCA performed on the stalagmite data. Although P was below detection in the dripwater data concentrations were significantly above the detection limit in the stalagmites, and also detectable in the total elemental analysis for the soil (Table 2). Whilst a bedrock or a soil component could not be identified there appears to be a clustering of the soil-derived dripwater elements in Ba and Cu with P (and additionally Si). This confirms the Ba concentration being a signature for soil-derived water in the dripwater samples. We hypothesised that the Mg/Sr ratio would not be constant over time and this is confirmed by the separation of these elements in PCA loadings plot (Figure 7). In the stalagmite, Sr contains little high-frequency variability compared to Mg, suggesting that the Sr does comprise a smoothed, bedrock-derived signal. The elements Ba and Mg are also separated confirming the complexity of the Mg signature. The source of the variability of Mg requires further investigation.

6. Conclusions

Through a series of short-term infiltration experiments the trace element geochemistry of dripwater was characterised in a semi-arid environment at Wellington Caves, Australia. Use of PCA on the combined trace element concentrations and PARAFAC scores (representing different fDOM pools) revealed two dominant components in the dripwater samples, a bedrock component and a soil component. The soil component, identified based on the contribution of the PARAFAC scores, also contained Ba, Cu, Mg, and Ni. The limestone bedrock component comprised Ca, Mg and Sr that are typical bedrock-derived elements and in addition Si, an element not normally associated with bedrock.

In contrast to temperate and alpine environments it is demonstrated that Mg can have contribution from the soil in addition to being solely bedrock-derived. It is notable that Ba, a typical bedrock-derived element was found to be soil-derived. These results were supported by soil and rock analysis with similar levels of Mg present in the soil and limestone samples, and Ba only detectable in the soil. Analysis of a stalagmite collected from this site supports these conclusions.

Our results demonstrate that infiltration water trace element composition at a particular semi-arid to arid site is likely to be site specific, and highly dependent on the existence of aeolian soil and salt deposits in the soil profile, and the soil salinity as a function of climate. Results from this study suggest that calibration of stalagmite trace element records should be on a site by site basis in these regions thus further research is needed from other sites. We show that Mg/Ca is highly unlikely to provide a unique or stationary paleoclimate proxy in these environments, and that the test of a constant ratio of Mg/Sr in stalagmites as proposed by Tremaine and Frolich (2013) is expected to fail.

In semi-arid to arid regions, recharge events are infrequent. Yet, the high rainfall amount required to overcome soil moisture deficit and evaporation can lead to recharge, and storage within the soil and the limestone bedrock which in turn can lead to episodes of both continuous and discontinuous dripping and subsequent speleothem formation. This was observed at our site. We have identified suites of trace elements that are indicative of soil and bedrock contact time and dripwater evolution. The observed behaviour of these trace element proxies in relation to speleothem paleoclimate reconstructions will form the basis of future work by the investigators.

Our conclusions have implications for the interpretation of speleothem trace element records in semi-arid to arid regions where $P<ET$. Typically, such sites are desert marginal and prone to aeolian deposition, and our results are relevant to any site where aeolian contributions to the soil might be significant. Overall, trace elements identified in this study in a semi-arid environment, cannot be assumed to follow the conventional interpretations that are more generally applicable in temperature climate zones. At these sites, models of Sr and Mg dripwater concentration as a single source, bedrock residence time signal, are unlikely to apply. Speleothem trace element records interpreted in this manner should be treated with caution.

7. Acknowledgements

We thank the staff at Wellington Caves for their support. Funding for this research was provided by the National Centre for Groundwater Research and Training, an Australian Government initiative, supported by the Australian Research Council and the National Water Commission. Thanks to Bruce Welsh and Philip Maynard from Sydney University Speleological Society for providing the survey map. Darrel Tremaine and two anonymous reviewers are thanked for their review comments.

8. References

Appelo, C.A.J., Postma, D., 2005. Geochemistry, Groundwater, and Pollution, second ed. A.A. Balkema, Rotterdam, 649 pp.

Bar-Matthews, M., Matthews, A., Ayalon, A., 1991. Environmental Controls of Speleothem Mineralogy in a Karstic Dolomitic Terrain (Soreq Cave, Israel). *The Journal of Geology* **99**, 189-207.

Borsato, A., Frisia, S., Fairchild, I.J., Somogyi, A., Susini, J., 2007. Trace element distribution in annual stalagmite laminae mapped by micrometer-resolution X-ray fluorescence: Implications for incorporation of environmentally significant species. *Geochimica et Cosmochimica Acta* **71**, 1494-1512.

Bowler, J.M., 1976. Aridity in Australia: age, origins and expressions in aeolian landformas and sediments. *Earth Science Reviews* **12,** 279-310.

Dainard, P.G., Guéguen, C., 2013. Distribution of PARAFAC modeled CDOM components in the North Pacific Ocean, Bering, Chukchi and Beaufort Seas. *Marine Chemistry* **157**, 216-223.

678 Dreybrodt, W., 1999. Chemical kinetics, speleothem growth and climate. *Boreas* **28**, 347-
679 356.
680 Eylem, C., Erten, H.N., Göktürk, H., 1990. Sorption-desorption behaviour of barium on
681 clays. *Journal of Environmental Radioactivity* **11**, 183-200.
682 Fairchild, I.J., Baker, A., 2012. Speleothem Science. Wiley-Blackwell 432pp.
683 Fairchild, I.J., Borsato, A., Tooth, A.F., Frisia, S., Hawkesworth, C.J., Huang, Y.,
684 McDermott, F., Spiro, B., 2000. Controls on trace element (Sr–Mg) compositions of
685 carbonate cave waters: implications for speleothem climatic records. *Chemical Geology*
686 **166**, 255-269.
687 Fairchild, I.J., Spotl, C., Frisia, S., Borsato, A., Susini, J., Wynn, P.W., Cauzid, J., 2010.
688 Petrology and geochemistry of annually laminated stalagmites from an Alpine cave (Obir,
689 Austria): seasonal cave physiology. *Geological Society, London, Special Publications* **336**,
690 295-321.
691 Fairchild, I.J., Treble, P.C., 2009. Trace elements in speleothems as recorders of
692 environmental change. *Quaternary Science Reviews* **28**, 449-468.
693 Frank, R., 1971. The clastic sediments of the Wellington Caves, New South Wales. *Helictite*
694 **9**, 3-26.
695 Frisia, S., Borsato, A., Drysdale, R.N., Paul, B., Greig, A., Cotte, M., 2012. A re-evaluation
696 of the palaeoclimatic significance of phosphorus variability in speleothems revealed by
697 high-resolution synchrotron micro XRF mapping. *Climate of the Past* **8**, 2039-2051.
698 Gingle, F.X., de Deckker, P., 2005. Clay mineral, geochemical and Sr-Nd isotopic
699 fingerprinting of sediments in the Murray-Darling fluvial system, southeast Australia,
700 *Australia Journal of Earth Sciences* **523**, 965-974.
701 Greene, R.S.B, Cattle, S.R., Mcpherson, A.A., 2009. Role of eolian dust deposits in
702 landscape development and soil degradation in southeastern Australia. *Australian Journal*
703 *of Earth Sciences* **56,** S55-65.
704 Hansen B.K., Postma D., 1995. Acidification, buffering, salt effects in the unsaturated zone
705 of a sandy aquifer, Klosterhede, Denmark. *Water Resources Research* **31,** 2795-2809.
706 Hartland, A., Fairchild, I.J., Lead, J.R., Borsato, A., Baker, A., Frisia, S., Baalousha, M.,
707 2012. From soil to cave: Transport of trace metals by natural organic matter in karst
708 dripwaters. *Chemical Geology* **304–305**, 68-82.
709 Hesse P.P., McTanish, G.H., 2003. Australian dust deposits: modern processes and the
710 Quaternary record. *Quaternary Sciences Reviews* **22**, 2007-2035.

711 Ishii, S.K., Boyer, T.H., 2012. Behavior of reoccurring PARAFAC components in fluorescent
712 dissolved organic matter in natural and engineered systems: a critical review.
713 *Environmental Science & Technology* **46**, 2006-2017.
714 Jex, C.N., Mariethoz, G., Baker, A., Graham, P., Andersen, M.S., Acworth, I., Edwards, N.,
715 Azcurra, C., 2012. Spatially dense drip hydrological monitoring and infiltration behaviour
716 at the Wellington Caves, South East Australia. *International Journal of Speleology* **41**,
717 285-298.
718 Johnson, B.D., 1975. The Garra Formation (early Devonian) at Wellington, N.S.W. *Journal*
719 *and Proceedings of The Royal Society of New South Wales* **108**, 111-118.
720 Lis, G., Wassenaar, I.L., Hendry, M.J., 2007. High-precision laser spectroscopy D/H and
721 18O/16O measurements of microliter natural water samples. *Analytical Chemistry* **80**,
722 287-293.
723 Mariethoz, G., Baker, A., Sivakumar, B., Hartland, A., Graham, P., 2012. Chaos and
724 irregularity in karst percolation. *Geophysical Research Letters* **39**, L23305.
725 McDonald, J., Drysdale, R., Hill, D., Chisari, R., Wong, H., 2007. The hydrochemical
726 response of cave drip waters to sub-annual and inter-annual climate variability,
727 Wombeyan Caves, SE Australia. *Chemical Geology* **244**, 605-623.
728 Norrish, K., Hutton, J.T., 1969. An accurate X-ray spectrographic method for the analysis of
729 a wide range of geological samples. *Geochimica et Cosmochimica Acta* **33**, 431-453.
730 Osborne, R.A.L., 2007. Cathedral Cave, Wellington Caves, New South Wales, Australia. A
731 multiphase, non-fluvial cave. *Earth Surface Processes and Landforms* **32**, 2075-2103.
732 Osborne, R.A.L., 2010. Rethinking eastern Australian caves. Geological Society, London,
733 Special Publications **346**, 289-308.
734 Roberts, M.S., Smart, P.L., Baker, A., 1998. Annual trace element variations in a Holocene
735 speleothem. *Earth and Planetary Science Letters* **154**, 237-246.
736 Siklósy, Z., Demény, A., Vennemann, T.W., Pilet, S., Kramers, J., Leél-Őssy, S., Bondár, M.,
737 Shen, C.-C., Hegner, E., 2009. Bronze Age volcanic event recorded in stalagmites by
738 combined isotope and trace element studies. *Rapid Communications in Mass Spectrometry*
739 **23**, 801-808.
740 Smith, C.L., Fairchild, I.J., Spötl, C., Frisia, S., Borsato, A., Moreton, S.G., Wynn, P.M.,
741 2009. Chronology building using objective identification of annual signals in trace
742 element profiles of stalagmites. *Quaternary Geochronology* **4**, 11-21.

Środoń, J., Drits, V.A., McCarty, D.K., Hsieh, J.C.C., Eberl, D.D., 2001. Quantitative X-ray diffraction analysis of clay-bearing rocks from random preparations. *Clays and Clay Minerals* **49**, 514-528.

Stedmon, C.A., Bro, R., 2008. Characterizing dissolved organic matter fluorescence with parallel factor analysis: a tutorial. *Limnology and Oceanography: Methods* **6**, 572-579.

Stedmon, C.A., Markager, S., Bro, R., 2003. Tracing dissolved organic matter in aquatic environments using a new approach to fluorescence spectroscopy. *Marine Chemistry* **82**, 239-254.

Sundqvist, H.S., Holmgren, K., Fohlmeister, J., Zhang, Q., Matthews, M.B., Spotl, C., Kornich, H., 2013. Evidence of a large cooling between 1690 and 1740 AD in southern Africa. *Nature Scientific Reports* **3**, 1767.

Tremaine, D.M., Froelich, P.N., 2013. Speleothem trace element signatures: A hydrological geochemical study of modern cave dripwaters amd farmed calcite. *Geochimica et Cosmochima Acta* DOI:10.1016/j.gca.2013.07.026.

Van Rampelbergh M., Fleitmann, D., Verheyden, S., Cheng, H., Edwards, L., De Geest, P., De Vleeschouwer, D., Burns, S.J., Matter, A., Claeys, P. and Keppens, E., 2013. Mid- to late Holocene Indian Ocean Monsoon variability recorded in four speleothems from Socotra Island, Yemen. *Quaternary Science Reviews* **65**, 129-142.

Wassenaar, L.I., Hendry, M.J., Chostner, V.L. and Lis G.P. 2008 High Resolution Pore Water δ2H and δ18O Measurements by H2O(liquid)-H2O(vapor) Equilibration, *Environmental Science and Technology* **42**, 9262–9267.

Wassenburg, J.A., A. Immenhauser, D.K. Richter, A. Niedermayr, S. Riechelmann, J. Fietzke, D. Scholz, K.P. Jochum, J. Fohlmeister, A. Schröder-Ritzrau, A. Sabaoui, D.F.C. Riechelmann, L. Schneider, J. Esper, 2013. Moroccan speleothem and tree ring records suggest a variable positive state of the North Atlantic Oscillation during the Medieval Warm Period. *Earth and Planetary Science Letters* **375**, 291-302.

Figure 1: (a) Plan view of Wellington Caves, New South Wales, with a boxed area indicating where the surface irrigation was performed (Adapted from Sydney University Speleology Society survey map 2006 – 2007). (b) Cross section from site survey indicating soil surface, bedrock profile and dripwater sites. (c) Location of study site in the Murray-Darling Basin of NSW showing possible dust sources indicated by arrows and climate zones, adapted from Bowler, 1976.

Figure 2: Time series of drip rates, deuterium, EC and concentrations of a selection of metal elements in response to infiltration events at Site 1 (red) and Site 2 (black).

Figure 3: PARAFAC scores over the course of the experiment for each factor at both sites. Factor 1 (F1: unprocessed soil-derived humic and fulvic like material); Factor 2 (F2: biogeochemically processed humic and fulvic like material; Factor 3 (F3: microbially-derived material). (N.B. no calibration was performed hence relative difference between factor scores do not necessarily represent the same relative differences in concentrations.)

Figure 4: Score plots of the principal component analysis of elemental and PARAFAC data over time at Site 1 and Site 2.

Figure 5: Ca versus Sr/Ca and Mg/Ca molar ratio for Site 1 and Site 2.

Figure 6: Trace element record from the top 2.6 mm of stalagmite C collected from Wellington Caves in 2011 A.D.

Figure 7: PCA loadings plot for components 1 and 2 of the Wellington stalagmite.

Table 1: Selected total elemental analysis results on dried soil and bedrock samples at the site. (BLD: below limit of detection)

Table 2: Elemental and PARAFAC scores contributions to PC1 (bedrock component) and PC2 (soil component).

Table1

	Soil	**Bedrock**
XRF analysis	**wt%**	**wt%**
Na_2O	0.20	0.01
MgO	0.57	0.33
Al_2O_3	13.33	0.07
SiO_2	52.84	0.11
P_2O_5	0.26	BLD
K_2O	1.73	BLD
CaO	2.19	57.49
Fe_2O_3	7.02	0.13
Loss on ignition	20.63	43.16
LA ICPMS analysis	**µg/g**	**µg/g**
Ba	165.5	0
Sr	70	118.2

Table2

	Site 1		Site 2	
	PC 1	PC 2	PC 1	PC 2
% explained variance	47.08	27.25	55.16	25.22
Ba	0.41	0.12	0.40	0.06
Ca	-0.003	0.49	0.01	0.24
Cu	0.17	-0.06	0.35	0.16
Mg	0.35	0.34	0.34	0.32
Ni	0.32	0.05	0.39	0.15
Si	-0.18	0.51	-0.15	0.54
Sr	0.02	0.58	0.14	0.58
PARAFAC1	0.41	-0.08	0.36	-0.26
PARAFAC2	0.42	-0.12	0.39	-0.20
PARAFAC3	0.43	-0.02	0.37	-0.22

Figure 1

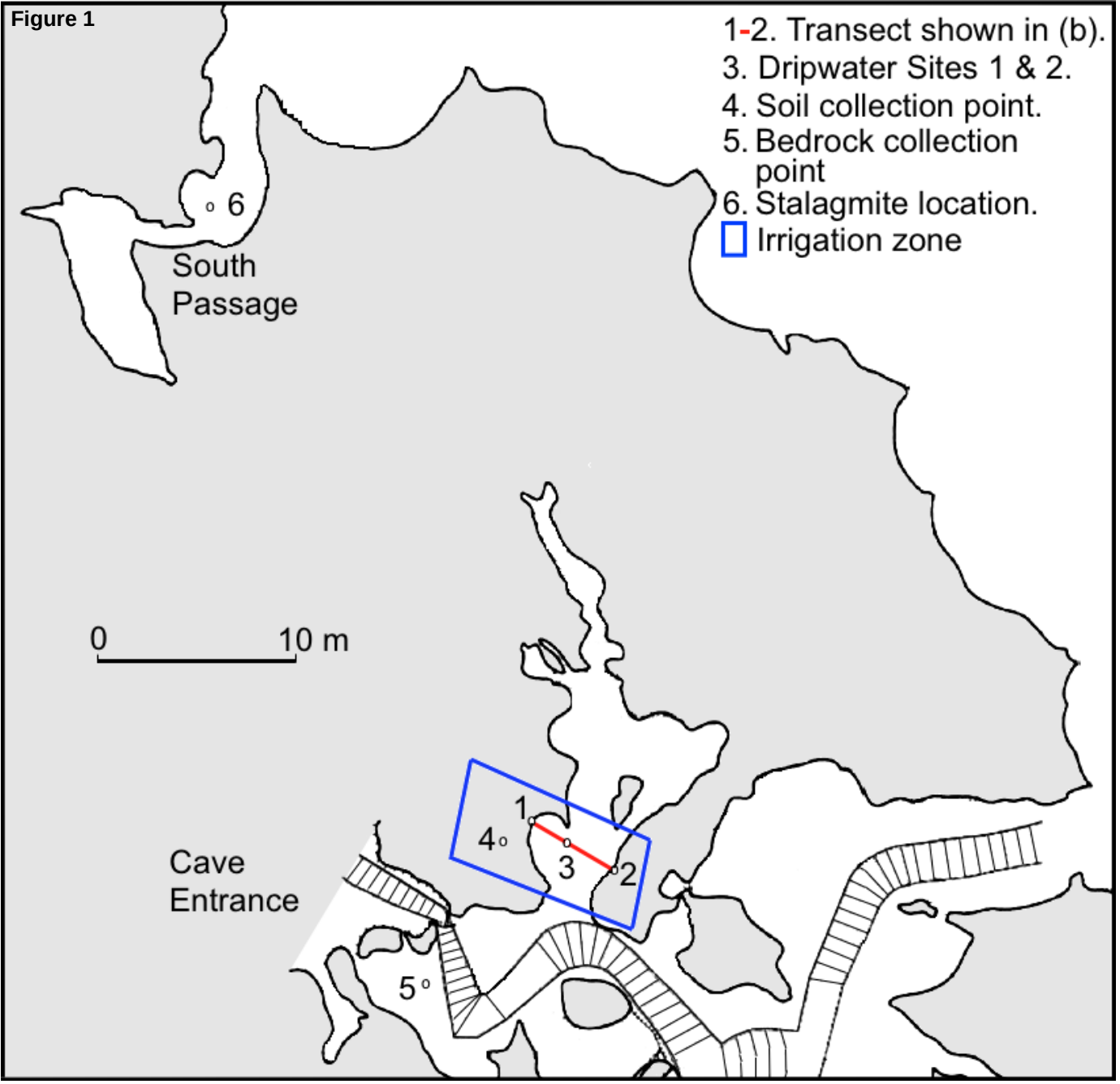
1-2. Transect shown in (b).
3. Dripwater Sites 1 & 2.
4. Soil collection point.
5. Bedrock collection point
6. Stalagmite location.
Irrigation zone
6
South Passage
0
10 m
Cave Entrance
1
2
3
4
5

(a)

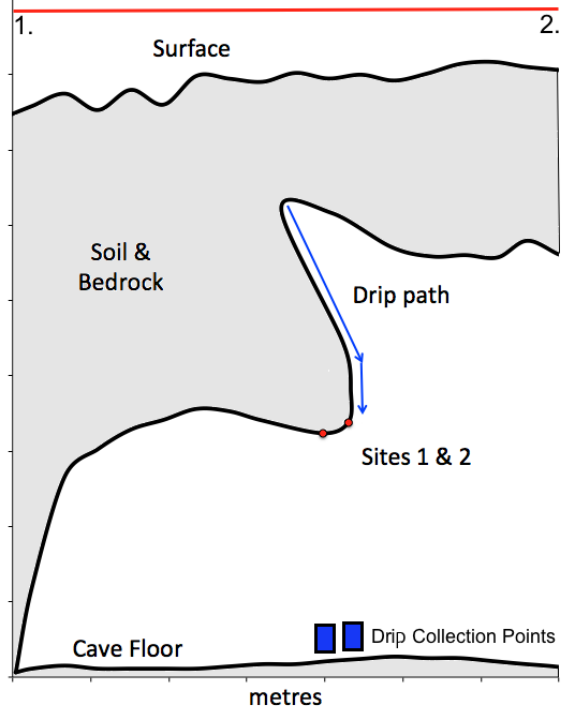
1.
2.
Surface
Soil & Bedrock
Drip path
Sites 1 & 2
Cave Floor
Drip Collection Points
metres

(b)

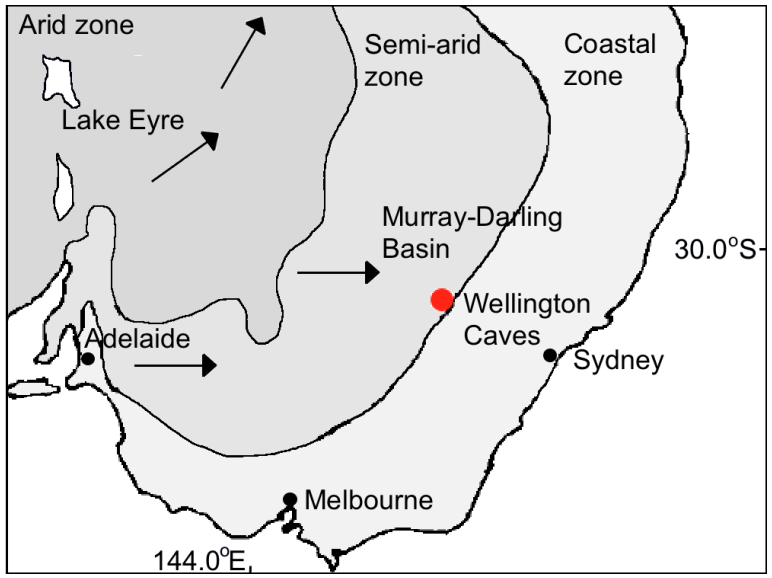
Arid zone
Semi-arid zone
Coastal zone
Lake Eyre
Murray-Darling Basin
30.0°S
Wellington Caves
Adelaide
Sydney
Melbourne
144.0°E

(c)

Figure 2

Click here to download high resolution image

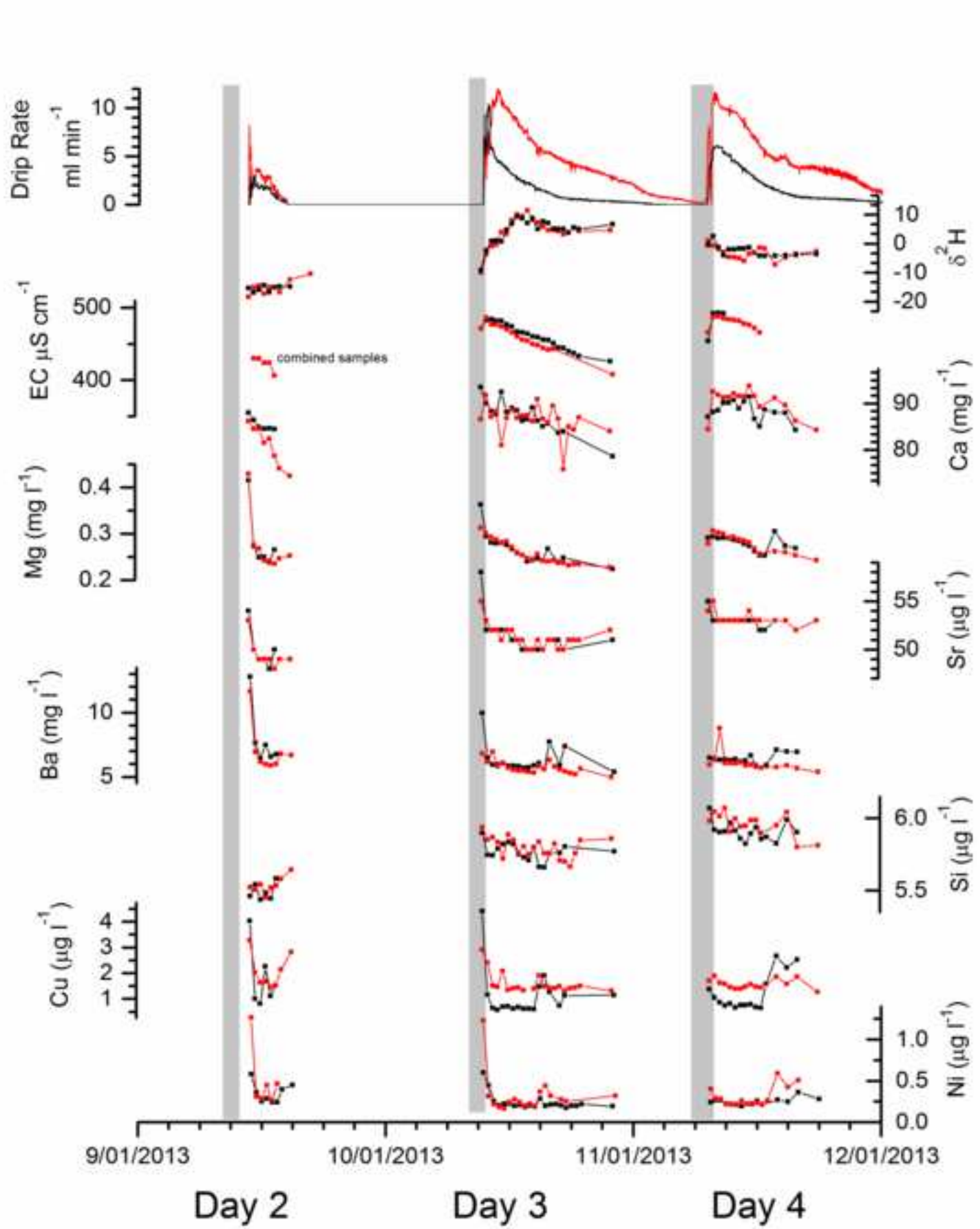

Figure 3

Click here to download high resolution image

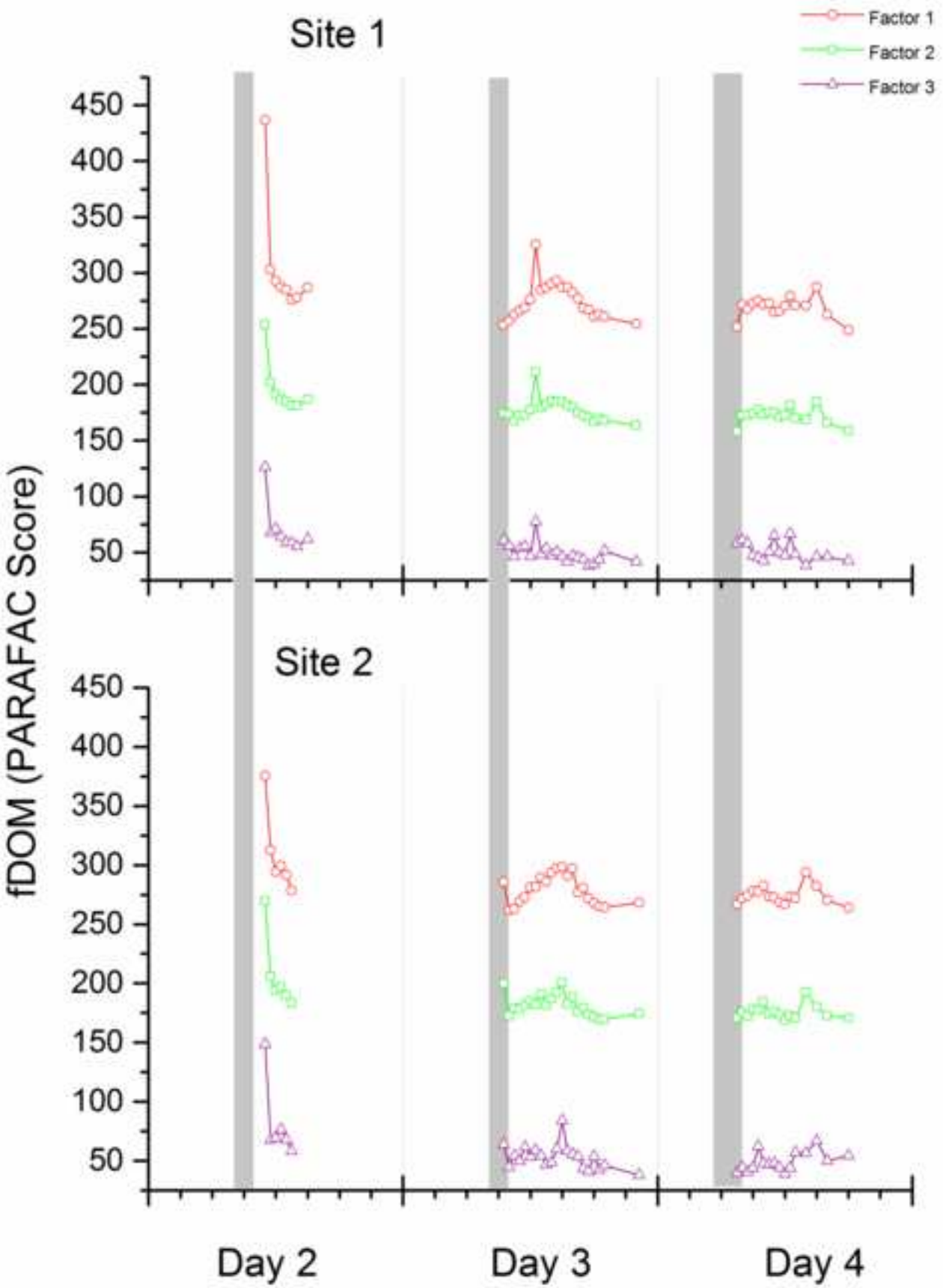

Figure 4

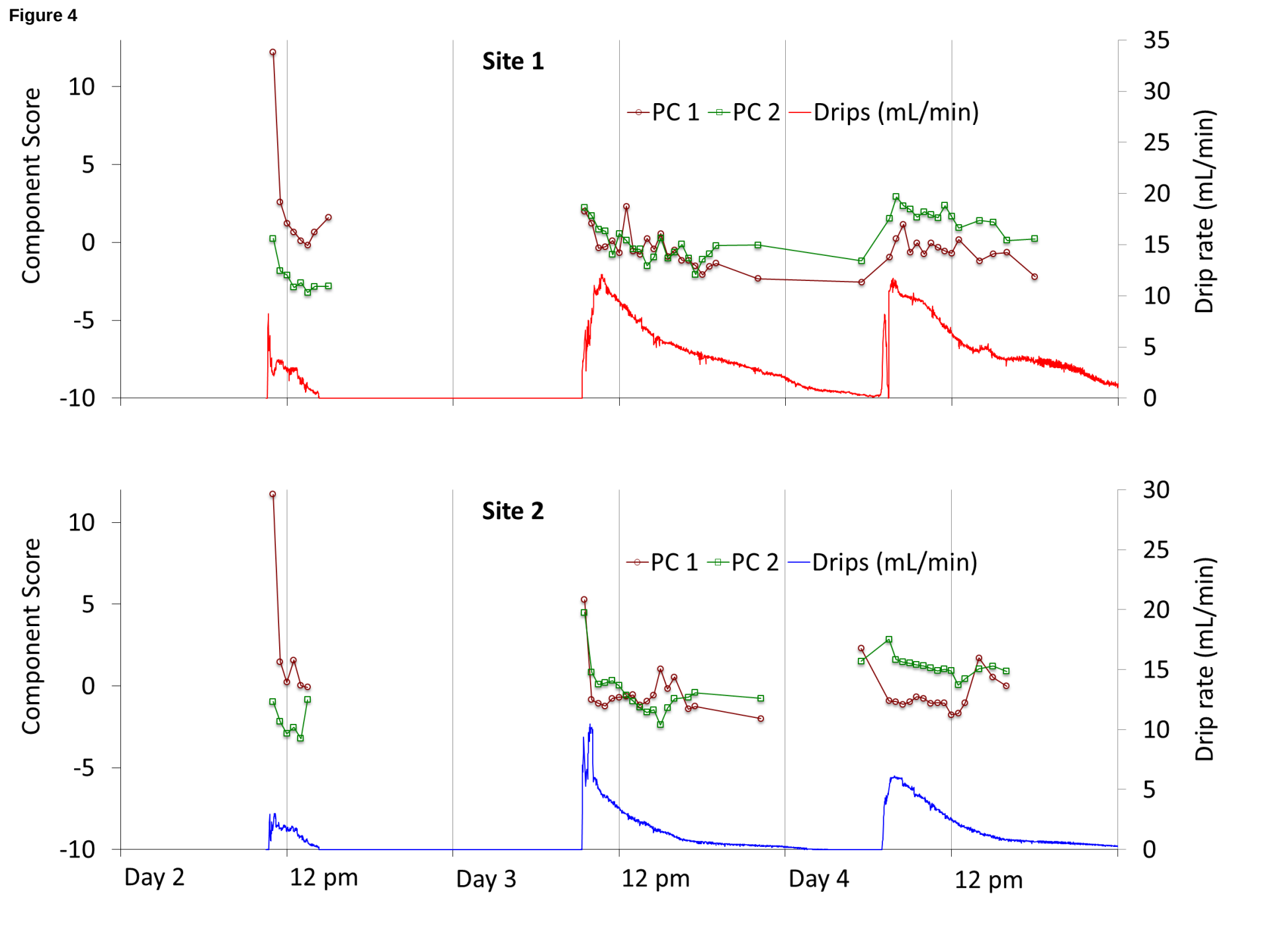
Site 1
PC 1
PC 2
Drips (mL/min)
Component Score
Drip rate (mL/min)
10
5
0
-5
-10
35
30
25
20
15
10
5
0
Site 2
PC 1
PC 2
Drips (mL/min)
Component Score
Drip rate (mL/min)
10
5
0
-5
-10
30
25
20
15
10
5
0
Day 2
12 pm
Day 3
12 pm
Day 4
12 pm

Figure 5

Click here to download high resolution image

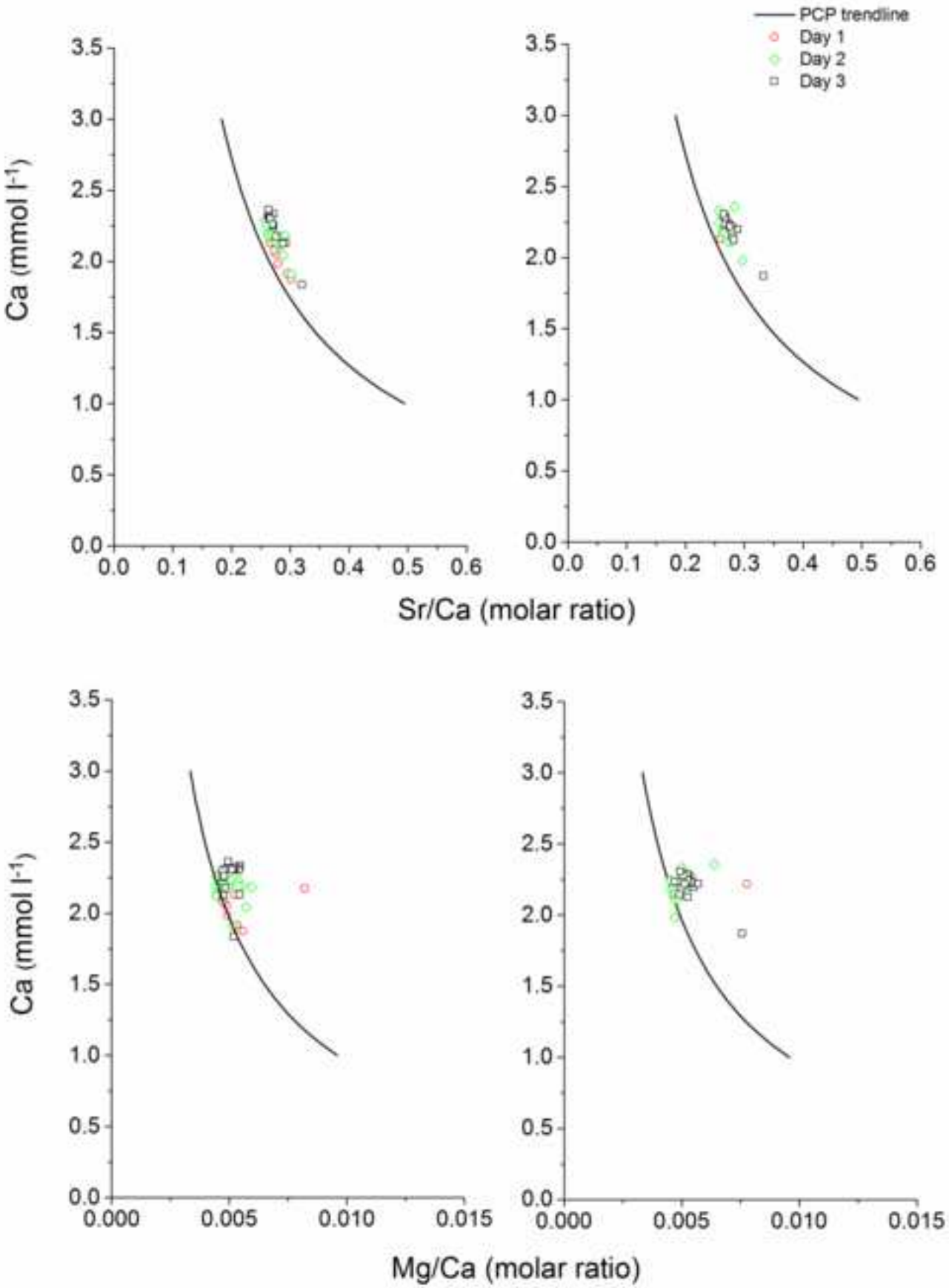

Figure 6

Click here to download high resolution image

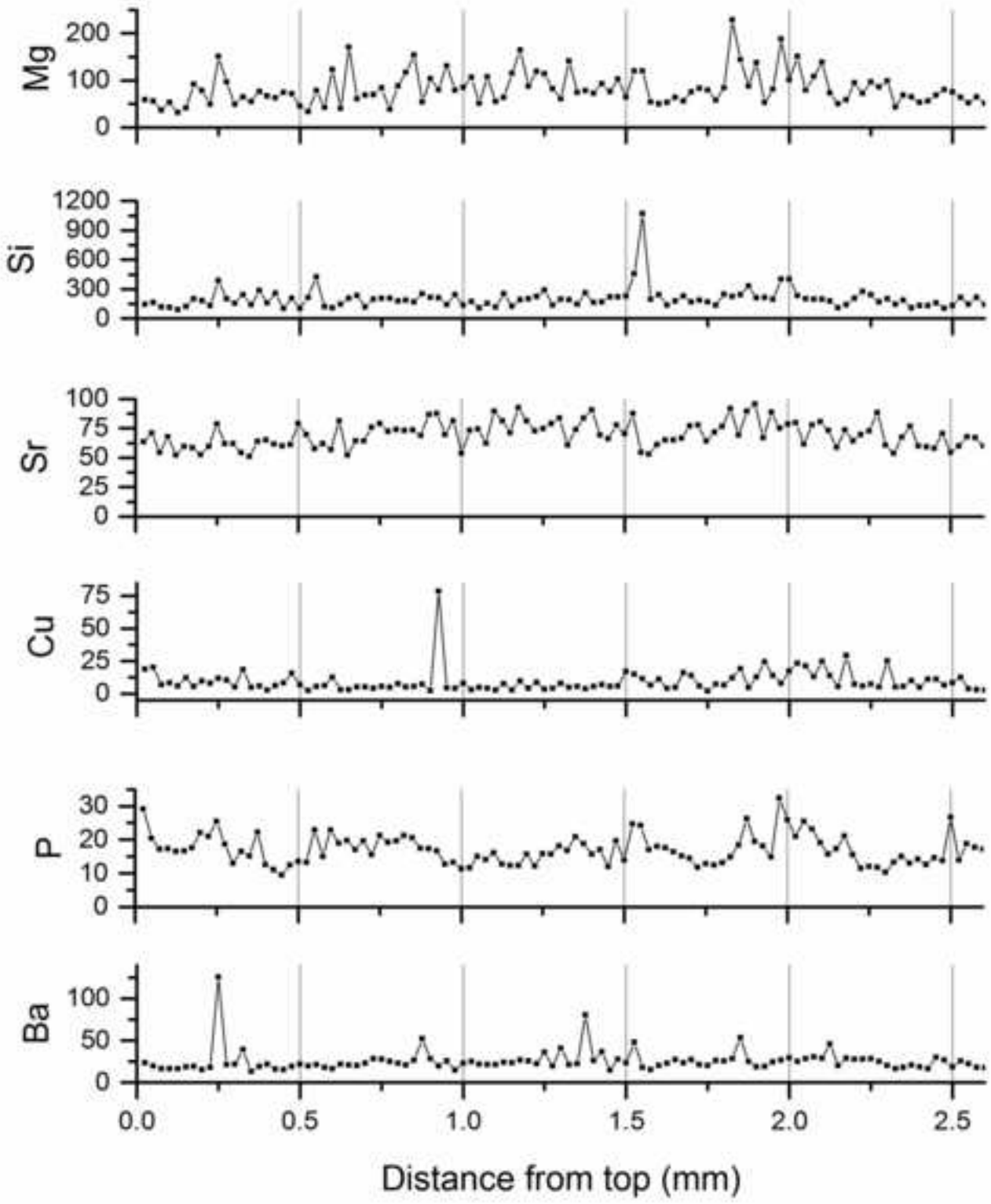

Figure 7

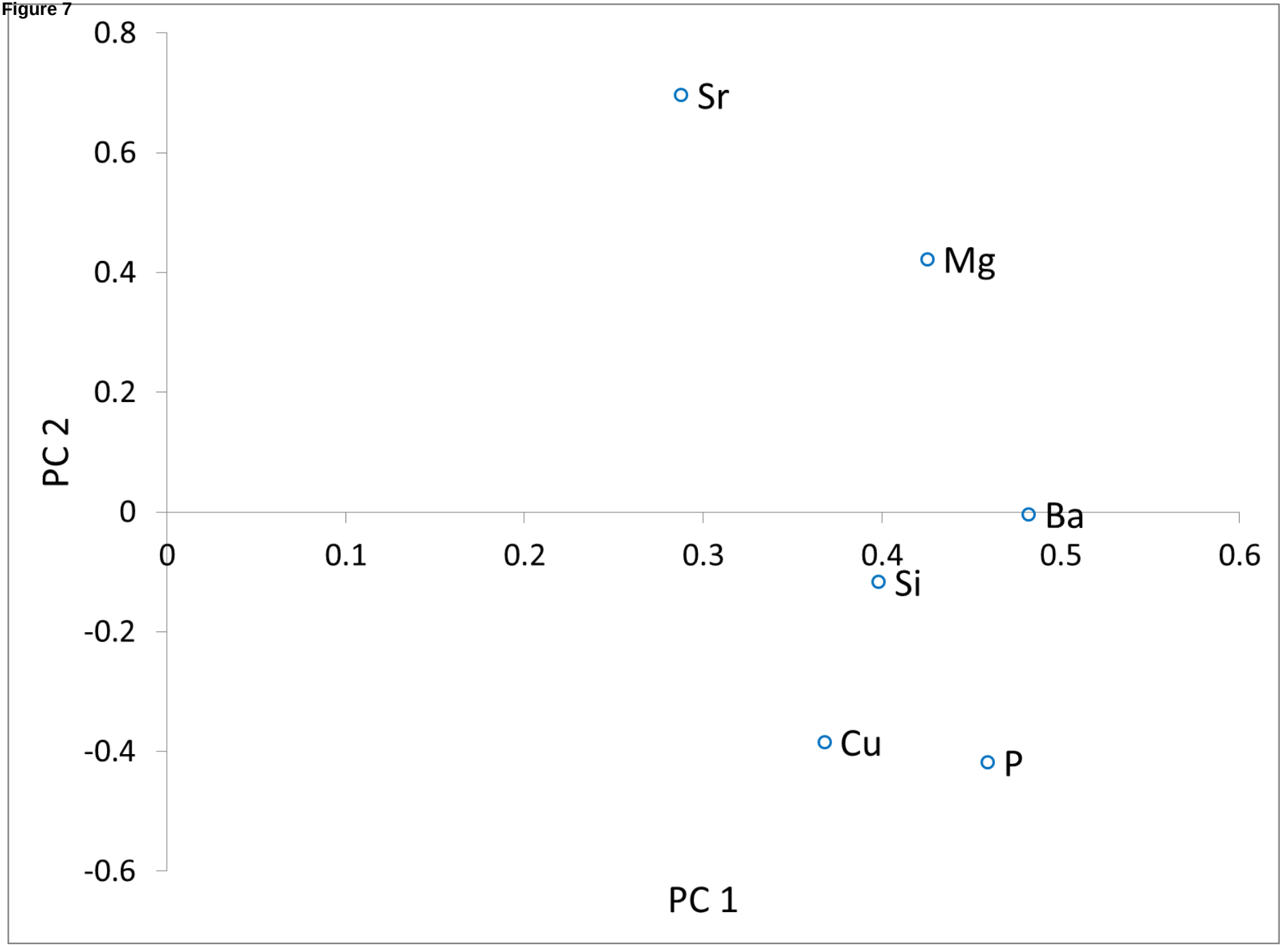

Supplementary Data

Click here to download Electronic Annex: Wello Manuscript (supporting).docx